IEEE Photonics Journal
An IEEE Photonics Society Publication

Multiwavelength Single-Longitudinal-Mode Brillouin–Erbium Fiber Laser Sensor for Temperature Measurements With Ultrahigh Resolution

Volume 7, Number 5, October 2015

Yi Liu
Mingjiang Zhang, Member, IEEE
Peng Wang
Lan Li
Yuncai Wang
Xiaoyi Bao

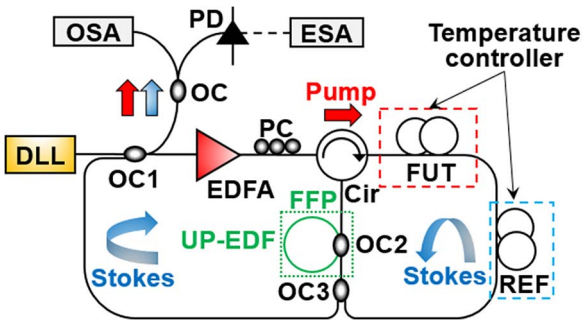

DOI: 10.1109/JPHOT.2015.2466511
1943-0655 © 2015 IEEE

Multiwavelength Single-Longitudinal-Mode Brillouin–Erbium Fiber Laser Sensor for Temperature Measurements With Ultrahigh Resolution

Yi Liu,[1,2] Mingjiang Zhang,[1,2] *Member, IEEE*, Peng Wang,[1,2] Lan Li,[2] Yuncai Wang,[1,2] and Xiaoyi Bao[3]

[1]Key Laboratory of Advanced Transducers and Intelligent Control Systems, Ministry of Education of Shanxi Province, Taiyuan 030024, China
[2]Institute of Optoelectronic Engineering, College of Physics and Optoelectronics, Taiyuan University of Technology, Taiyuan 030024, China
[3]The Fiber Optics Group, Department of Physics, University of Ottawa, Ottawa ON, Canada

DOI: 10.1109/JPHOT.2015.2466511

Manuscript received August 4, 2015; accepted August 6, 2015. Date of publication August 10, 2015; date of current version August 31, 2015. This work was supported in part by the National Natural Science Foundation of China under Grant 61377089, Grant 61205142, Grant 61527819, and Grant 611227016; by the Program for the Top Young Academic Leaders of Higher Learning Institutions of Shanxi (TYAL) under Grant 2012lfjyt08; by the Key Science and Technology Research Project Based on Coal of Shanxi Province under Grant MQ2014-09; by the National Science and Technology Infrastructure Program of the Ministry of Science and Technology of Shanxi Province, China, under Grant 2013091021; and by the Program of the Key Laboratory of Opto-Electric Information Technology, Ministry of Education (Tianjin University), under Grant 2014KFKT021. Corresponding author: M. Zhang (e-mail: zhangmingjiang@tyut.edu.cn).

Abstract: A multiwavelength single-longitudinal-mode (SLM) Brillouin–erbium fiber laser sensor with ultrahigh resolution is proposed and investigated experimentally. The one short common cavity with 50 m of single mode fiber (SMF) as the fiber under test and 100 m of SMF as the reference can effectively reduce the external perturbations and the cost. With the configuration that uses a fiber Fabry–Pérot (FFP) filter, every Stokes wavelength maintains SLM status, which can lead to the higher temperature resolution. In the experiment, 3.104 MHz/°C sensitivity of the third-order Stokes wavelength is demonstrated, which is three times that of the first-order Stokes wavelength. A less-than 0.2 °C temperature error is obtained for every Stokes wavelength. In contrast, with a beat frequency linewidth of a different order Stokes wavelength, approximately 10^{-6}°C ultrahigh resolution in the short term is acquired at the third-order Stokes wavelength. This proposal can provide a feasible temperature sensing scheme with high sensitivity, high precision, and low-frequency detection.

Index Terms: High-order Stokes wavelength, multiwavelength fiber laser, temperature sensor.

1. Introduction

Over the past few decades, fiber laser sensors have demonstrated high signal-to-noise ratios (SNRs) and narrow linewidths; such characteristics indicate that these sensors have an inherent high resolution [1], [2]. Such sensors have been applied in accelerometers [3], acoustic microphones [4], strain sensors [5] and temperature sensors [6]–[12]. In particular, more attention has

been given to the measurement of temperature, which is one of the seven fundamental physical quantities. Currently, there are three main types of fiber laser temperature sensors, including a single-longitudinal mode fiber laser (SLM-FL) sensor [6]–[8], a multilongitudinal mode fiber laser (MLM-FL) sensor [9], [10] and a multiwavelength fiber laser (MW-FL) sensor [11], [12]. On the one hand, for the SLM-FL and MW-FL sensors, wavelength matched fiber Bragg gratings (FBGs) are used as wavelength selectors and sensor elements. In this case, the temperature information is achieved by measuring the wavelength shift under different temperatures in the optical domain or the power variation at a specific wavelength on the grating's slope. In addition, this type of fiber laser sensor is limited by the tuning speed of the filter, the sensitivity of the detector, and the complexity of the optical interferometer, and the signal is detected by mixing with an additional tunable laser source. On the other hand, for the MLM-FL sensor, the temperature difference can be easily detected by measuring the beat frequency generated by any two longitudinal modes. Because the disturbance can be reduced, the beat frequency can be dynamically stable. Thus, the higher the detected beat frequency is, the better the sensitivity is. However, although the 74th-order mode (1581.7 MHz) [9] is detected, only sensitivity at the scale of 1 kHz/°C is obtained.

Recently, based on the Brillouin scattering (BS) effect in optical fibers, Yang *et al.* [13] proposed a novel dual-frequency Brillouin fiber laser (DF-BFL) for microwave generation; temperature sensing was realized based on this configuration, which has two cavities with different types of fiber. According to the linear relationship between the Brillouin frequency shift and temperature, the sensing information can be obtained by measuring the beat frequency shift as the temperature of the DF-BFL. This method may provide a stable fiber laser sensor with 1.015 MHz/°C sensitivity. Compared to the DF-BFL, the use of the multiwavelength Brillouin–erbium fiber laser (MW-BEFL) [14]–[19] based on the cascade BS effect and the linear gain from EDF could be an advanced method. Iezzi [20] and Zhang [21] realized temperature measurements with sensitivities of $\sim$7 MHz/°C and 13.08 MHz/°C by using the 6th-order and the 12th-order Stokes shifts with BS of two MW-BEFLs, respectively. However, due to the kilometer-scale laser cavity length (10 km and 27 km), the external perturbations became the main effect factor for the temperature error, and the MLM operation status limited the improvement of the system resolution.

In this paper, a SLM MW-BEFL with a short cavity used as the temperature sensor is proposed and investigated experimentally. As the configuration of the DF-BFL, a 50 m long SMF is used as the fiber under test (FUT), and a 100 m long SMF is used as the reference fiber (REF). This one short common cavity setup can effectively reduce the external perturbations and cost. With the configuration that uses a fiber Fabry–Pérot (FFP) filter, every Stokes wavelength of the MW-BEFL maintains SLM status. In contrast, with beat frequency linewidths of different order Stokes wavelengths, approximately 10^{-6} °C ultra-high resolution in the short-term (linewidth) is acquired at the third-order Stokes wavelength. To our knowledge, these results represent the best temperature resolution to date.

2. Experimental Setup and Principle

The experimental setup of the MW-BEFL is shown in Fig. 1. The pump light from a Dense Light laser (DLL) with a 10 kHz linewidth and a maximum output power of 10 dBm travels through a 50/50 optical coupler (OC1). Next, the light is first amplified by the EDFA. To achieve maximum Brillouin gain, the polarization of the pump is kept parallel to the Stokes polarization by a polarization controller (PC). The pump is injected into the ring cavity (RC) clockwise by an optical circulator (Cir) and then passes through the cavity with only one roundtrip. The RC is constructed with one 50-m FUT, another 100-m REF, an OC3 and a FFP filter. This 50 m and 100 m configuration guarantees a sufficient amount of BS pump power for the FUT and the REF [19] when a different temperature is configured. The FFP filter is composed of a 50/50 polarization insensitive OC2 and a 10 m unpumped erbium-doped fiber (UP-EDF), which acts as a saturable absorber (SA). The fiber type of the FUT and REF is standard G.652 SMF, and the FFP filter is used to

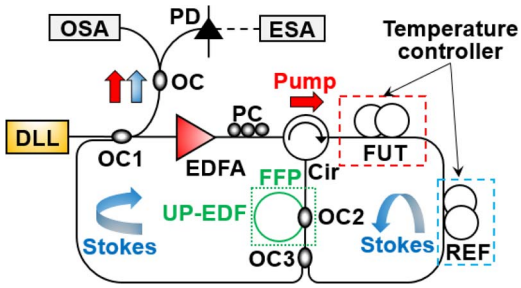

Fig. 1. Experimental Setup. DLL: Dense Light laser; OC: optical coupler; PC: polarization controller; Cir: circulator; FUT: fiber under test; REF: reference fiber; FFP: fiber Fabry–Pérot; UP-EDF: unpumped erbium-doped fiber; PD: photodetector; OSA: optical spectrum analyzer; ESA: electric spectrum analyzer.

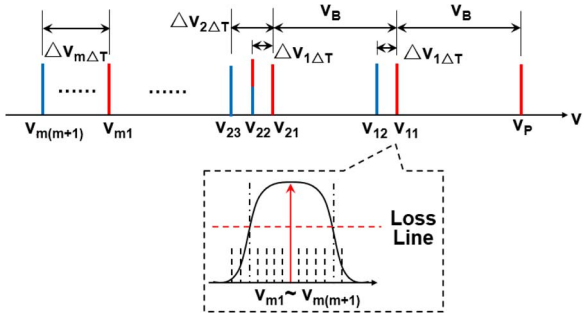

Fig. 2. Principle of the high-order Stokes wavelength for temperature sensing with a ΔT temperature difference.

keep every Stokes wavelength in SLM status. When the EDFA power is higher than the threshold of BS, 10% (OC3) of the Stokes returns back to OC1 and is amplified likewise by the EDFA clockwise. Next, the light is injected into the RC to excite the next order Stokes, and the rest circulates (90%) in the RC with multiple roundtrips anticlockwise. The output of the laser was monitored by an electric spectrum analyzer (ESA) with a 1 Hz frequency resolution and a photodetector (PD) with a 26.5 GHz bandwidth. For the convenience of temperature measurement, the FUT and REF are enclosed in two similar temperature controller systems with the following characteristics: 0.2 °C resolution, a 5 $\sim$ 60 °C range, and no strain. In this experiment, the temperature of the REF is fixed at 20 °C, and that of the FUT is adjusted from 20 °C to 50 °C.

2.1. Temperature Sensing by Detecting the High-Order Stokes Wavelength

Fig. 2 shows the high-order Stokes wavelength sensing principle based on the cascade BS effect for temperature measurement. The frequency shift ν_B with respect to the pump is given by $\nu_B = (2V_A/c)\lambda_P$ [14]–[19], where V_A is the acoustic velocity in the medium, c is the vacuum-light velocity, and λ_P is the pump wavelength. ν_B is approximately 10 GHz at a 1550 nm wavelength.

We can obtain the relationship between ν_{m1} at room temperature and $\nu_{m(m+1)}$ for the ΔT temperature difference of the mth-order Stokes wave [13], [20]–[23]

$$\nu_{m1} = \nu_{(m-1)1} + \nu_B = \cdots = \nu_P + m\nu_B \tag{1}$$

$$\nu_{m(m+1)} = \nu_{(m-1)m} + \nu_B + \Delta\nu_{\Delta T} = \cdots = \nu_P + m\nu_B + \Delta\nu_{m\Delta T} \tag{2}$$

$$\Delta\nu_{m\Delta T} = c_{Bm}\Delta T = \cdots = mc_{B1}\Delta T \tag{3}$$

where ν_P is the optical frequency of the pump beam, m is the order number of the Stokes wave $(m = 1, 2, 3 \ldots)$, and $\Delta\nu_{m\Delta T}$ and c_{Bm} are the Brillouin frequency difference and the temperature coefficient of the mth-order Stokes wave, respectively; i.e., the frequency shift with temperature and the temperature coefficient of the mth-order Stokes are m-times greater than those of the first-order Stokes.

2.2. SLM Principle

The inset of Fig. 2 shows the principle of SLM operation using the FFP filter. According to the Vernier effect [24], [25], the effective free spectral range $(\mathrm{FSR_{eff}})$ of the MW-BEFL with the FFP filter is $\mathrm{FSR_{eff}} = y_1\mathrm{FSR_{RC}} = y_2\mathrm{FSR_{FFP}}$, where $\mathrm{FSR_{RC}}$ and $\mathrm{FSR_{FFP}}$ are the FSR values of the RC filter and the FFP filter, respectively, and y_j $(j = 1, 2)$ is an integer. The FSR values of the FUT, REF and FFP are 2 MHz, 4 MHz, and 20 MHz, respectively, while $\mathrm{FSR_{eff}} = 20$ MHz. Thus, when $\mathrm{FSR_{eff}}$ exceeds the Brillouin gain bandwidth $(\Delta\nu_B = 20$ MHz$)$ and gain is greater than loss, the laser mode (range from ν_{m1} to $\nu_{m(m+1)}$) oscillates only at a frequency that satisfies the resonant conditions of the RC and FFP simultaneously. Thus, higher temperature resolution can be obtained in comparison to the previously reported structure [20], [21].

2.3. Temperature Resolution by Detecting the High-Order Stokes Wavelength

The temperature resolution depends on the short-term (linewidth) and the long-term stability of the high-order Stokes wavelength. On the one hand, the relation connecting the mth-order Stokes linewidth $\Delta\nu_m$ of the MW-BEFL and the pump laser linewidth is given by [26]

$$\Delta\nu_m = \frac{\Delta\nu_{m-1}}{(1+\gamma_A/\Gamma_C)^2} = \cdots = \frac{\Delta\nu_1}{(1+\gamma_A/\Gamma_C)^{2^{m-1}}} = \frac{\Delta\nu_p}{(1+\gamma_A/\Gamma_C)^{2^m}} \tag{4}$$

where $\gamma_A = \pi\Delta\nu_B$ is the damping rate of the acoustic wave, $\Gamma_C = -c \ln R/nL_t$ is the cavity loss rate, and L_t is the total cavity length. In this case, the relationship between the temperature resolution T_{Rm} of the m-order Stokes wavelength and the temperature resolution T_{R1} of the first-order Stokes wavelength can be written as

$$T_{Rm} = \frac{\Delta\nu_m}{c_{Bm}} = \frac{1}{m(1+\gamma_A/\Gamma_C)^{2^{m-1}}}\left(\frac{\Delta\nu_1}{c_{B1}}\right) = \frac{T_{R1}}{m(1+\gamma_A/\Gamma_C)^{2^{m-1}}}. \tag{5}$$

Thus, the higher the order of the Stokes wavelength is, the better the temperature resolution is. In other words, the temperature measurement resolution can be enhanced by $m(1+\gamma_A/\Gamma_C)^{2^{m-1}}$-times. On the other hand, among the three main effects determining the frequency stability of MW-BEFL [22], [23], the temperature effect mainly influences the Brillouin gain spectrum. The temperature range ΔT with two consecutive mode hops for the MW-BEFL is expressed by

$$\Delta T \approx \frac{FSR_{\min}}{\left[\nu_B\left(\frac{1}{\nu_B}\frac{\partial\nu_B}{\partial T} + \frac{1}{n}\frac{\partial n}{\partial T} + \frac{1}{L_t}\frac{\partial L_t}{\partial T}\right)\right]} \tag{6}$$

where $(1/L_t)(\partial L_t/\partial T) = 10^{-6}$ °C is length fluctuation coefficient with SMF temperature, and $\partial\nu_B/\partial T = 1.2$ MHz °C is the Brillouin frequency shift with temperature at 1550 nm.

3. Experimental Results and Discussions

3.1. Threshold Measurement of the MW-BEFL Sensor

First, the threshold of every Stokes wavelength is measured using an optical spectrum analyzer (OSA) with a spectral resolution of 0.02 nm. Fig. 3(a) shows the multiwavelength generation of the MW-BEFL, and Fig. 3(b) shows the output power of every Stokes wavelength and the total output power versus the EDFA power. We can observe three output power states

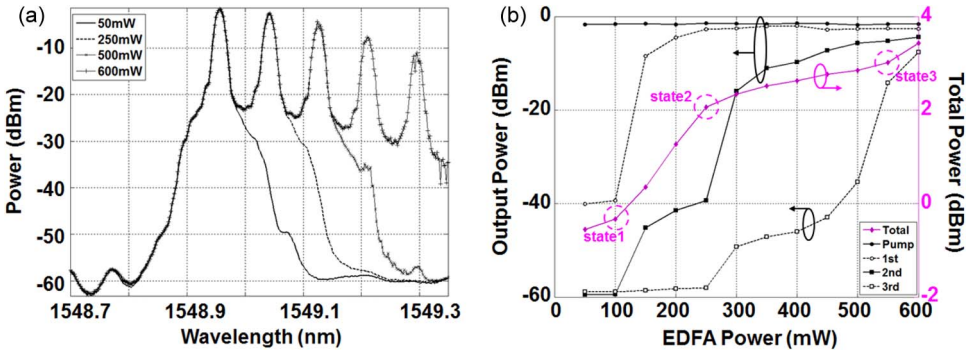

Fig. 3. (a) Multiwavelength generation of the MW-BEFL and (b) relationship between EDFA power and output power of every Stokes wavelength and total output power.

measured every 50 mW from 50 mW to 600 mW. First, the DLL is fixed at a 1548.95 nm wavelength and a 0 dBm power, and the EDFA power is fixed at 50 mW. In this case, there is no Stokes wavelength; i.e., the EDFA power did not exceed the threshold of the first Stokes line. When the EDFA power reaches 100 mW, which is the threshold of the first-order Stokes wavelength, the total power begins to linearly increase rapidly. For an EDFA power of 250 mW, the first-order Stokes wavelength with -6.05 dBm reaches saturation. Although the second-order Stokes wavelength is generated, the total power increases slowly because of the 8 dB power difference between the former and the latter. When the EDFA power is increased to 500 mW, the first-order and the second-order Stokes wavelengths are observed. By increasing the EDFA power further to 600 mW, four Stokes wavelengths are generated because of the cascaded BS effect. At the same time, due to the generation of the third-order Stokes wavelength, the total power begins to increase again.

3.2. Temperature Measurement Using Different Order Stokes Waves

According to the threshold measurement results of the MW-BEFL sensor, the relationships between the temperature difference and the different Stokes wavelengths are also measured for different EDFA power levels (see Fig. 4). The circular and square dots represent real frequency values, including $\nu_{12} - \nu_P$, $\nu_{22} - \nu_P$, $\nu_{23} - \nu_P$, and $\nu_{34} - \nu_{31}$, measured at a FUT temperature from 20 °C to 50 °C every 5 °C and at a REF temperature of 20 °C under 250 mW, 500 mW, and 600 mW. The x-axis is $\Delta T = T_{\mathrm{FUT}} - T_{\mathrm{REF}}$, and the black solid lines are the results of linear fits using a least squares fitting method. The fitting lines show the temperature dependences of the frequency shift of the FUT and the REF. As seen from the solid line, all the beat frequencies are linear with respect to temperature, while the frequency of $\nu_{22} - \nu_P$ is used for comparison.

The temperature elevation coefficient of the first-order Stokes wavelength is 1.036 MHz/°C [see Fig. 4(a)], which is reasonably close to the previously reported value of 1.2 MHz/°C [27]. The temperature elevation coefficient of the second-order Stokes wavelength is 2.006 MHz/°C [shown in Fig. 4(b)], which is twice as much as that of the first-order Stokes wavelength. The coefficient of the comparison frequency $\nu_{22} - \nu_P$ is equal to that of $\nu_{12} - \nu_P$. Similarly, the temperature elevation coefficient of the third-order Stokes wavelength is 3.104 MHz/°C [shown in Fig. 4(c)], which is three-times greater than that of the first-order Stokes wavelength. The measurement values are almost exactly the same as the theoretical value described by (3) and are very close to the reported values of 2.18 MHz/°C, 2.27 MHz/°C, and 3.29 MHz/°C [20], [21].

Meanwhile, the SLM operation of every Stokes wavelength is observed for a FUT temperature of 50 °C and a REF temperature of 20 °C. Fig. 5(a) shows the beat frequency spectra of $\nu_{11} - \nu_P$ and $\nu_{12} - \nu_P$ with 250 mW of EDFA power. Fig. 5(b) shows the beat frequency spectra of $\nu_{21} - \nu_P$, $\nu_{22} - \nu_P$, and $\nu_{23} - \nu_P$ with 500 mW of EDFA power. Fig. 5(c) shows the beat frequency spectra of $\nu_{34} - \nu_{31}$, f_2 (which is the sum of $\nu_{23} - \nu_{21}$, $\nu_{33} - \nu_{31}$, and $\nu_{34} - \nu_{32}$),

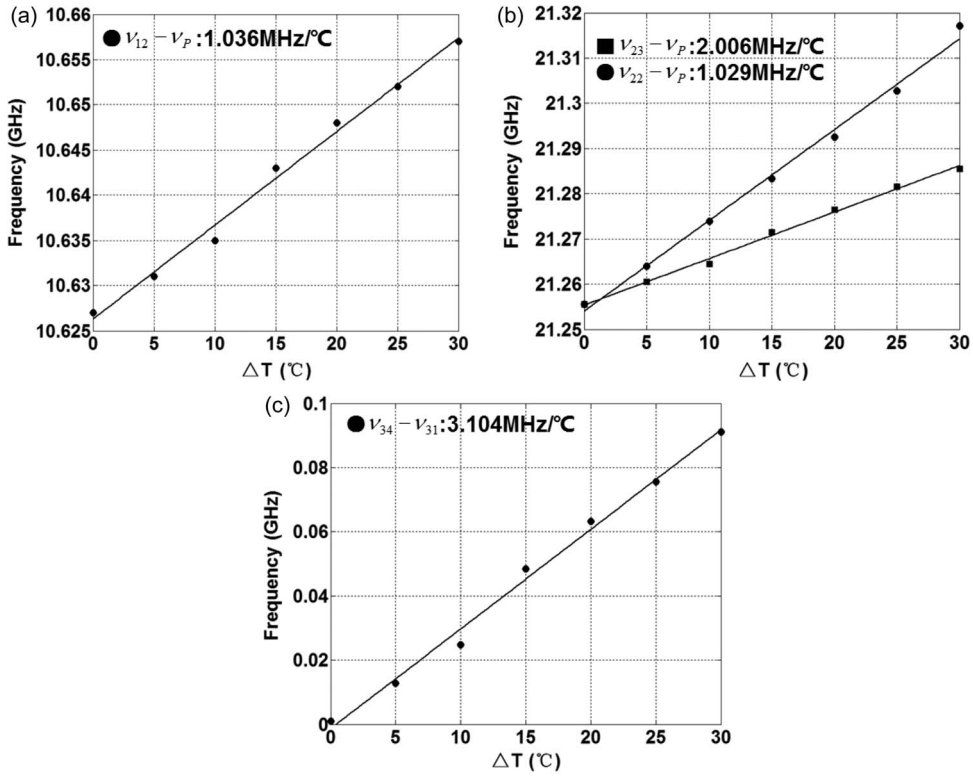

Fig. 4. Temperature difference $\Delta T = T_{FUT} - T_{REF}$ and beat frequency shift relationship for (a) $\nu_{12} - \nu_P$, (b) $\nu_{22} - \nu_P$, $\nu_{23} - \nu_P$, and (c) $\nu_{34} - \nu_{31}$.

and f_1 (which is the sum of $\nu_{12} - \nu_{11}$, $\nu_{22} - \nu_{21}$, $\nu_{23} - \nu_{22}$, $\nu_{32} - \nu_{31}$, $\nu_{33} - \nu_{32}$, and $\nu_{34} - \nu_{33}$) with 600 mW of EDFA power. Every Stokes wavelength remains in SLM operation and maintains a reasonable frequency spacing with 30.41 MHz, 29.71 MHz, 31.85 MHz, 31.23 MHz, 36.75 MHz, and 33.52 MHz. From a comparison of the results, the noise power of Fig. 5(a) is the lowest, approximately −90 dBm, which is less than the −85 dBm of Fig. 5(b) and −80 dBm of Fig. 5(c). The reason for this result is the existence of some invalid beat frequencies resulting from the idler frequency, such as ν_{22}, ν_{32}, and ν_{33}, which reduce the power conversion efficiency and generate the idler beat frequency, such as $\nu_{22} - \nu_P$, the sum of $\nu_{33} - \nu_{31}$ and $\nu_{34} - \nu_{32}$, and the sum of $\nu_{22} - \nu_{21}$, $\nu_{23} - \nu_{22}$, $\nu_{32} - \nu_{31}$, $\nu_{33} - \nu_{32}$, and $\nu_{34} - \nu_{33}$. Furthermore, because each idler beat frequency has a different polarization, the frequencies of f_1 and f_2 are not completely in the SLM status.

3.3. Temperature Error and Resolution of the MW-BEFL Sensor

Fig. 6 show the beat frequency and peak power stability of the frequencies $\nu_{11} - \nu_P$, $\nu_{21} - \nu_P$ and $\nu_{34} - \nu_{31}$ measured every 3 min in 1 h at a REF temperature of 20 °C and a FUT temperature of 50 °C (in the long-term). It is shown that the frequency and the power are stabilized with a ±0.2 MHz frequency fluctuation and a ±0.1 dB power fluctuation. The frequency shift corresponds to a temperature error of 0.2 °C. According to (6), a 0.2 °C ($< \Delta T \approx 1.89$ °C) resolution of the temperature controller system cannot lead to mode hopping, where $FSR_{min} = 2$ MHz for the 100 m cavity length is taken. In addition, the 0.2 °C temperature error is consistent with the resolution of the temperature controller system; i.e., the temperature error of every Stokes wavelength is less than 0.2 °C.

To exactly measure the temperature resolution, we must take the linewidth of the pump into consideration. Next, the beat frequency linewidths of f_1, f_2, and $\nu_{34} - \nu_{31}$ are measured using

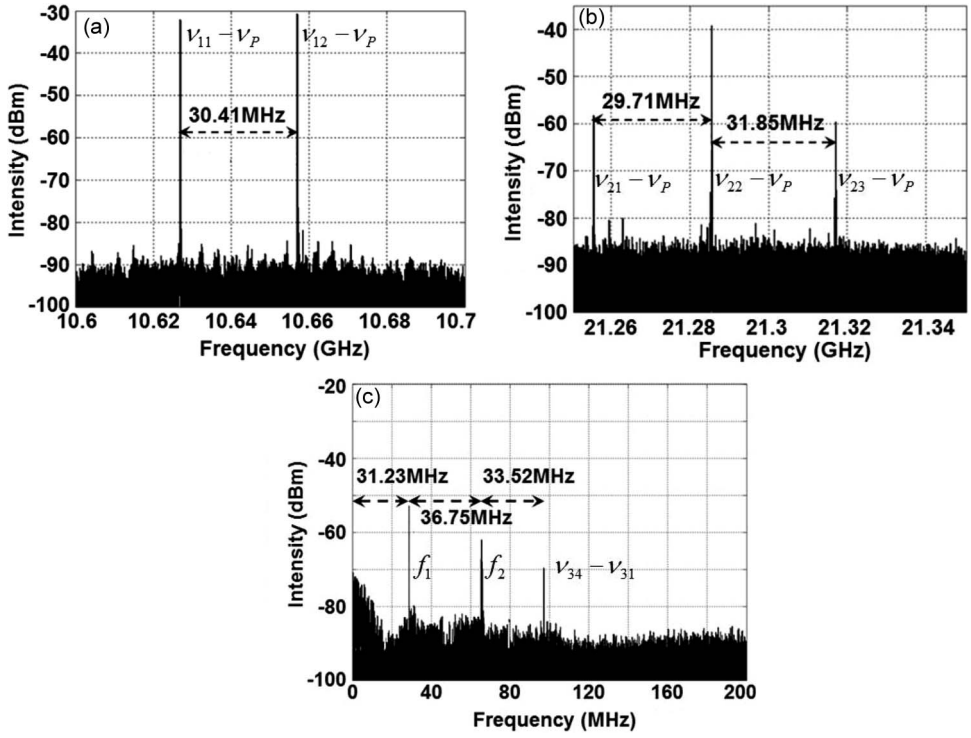

Fig. 5. Beat frequency spectra for a FUT temperature of 50 °C and a REF temperature of 20 °C with (a) 250 mW, (b) 500 mW, and (c) 600 mW of EDFA power.

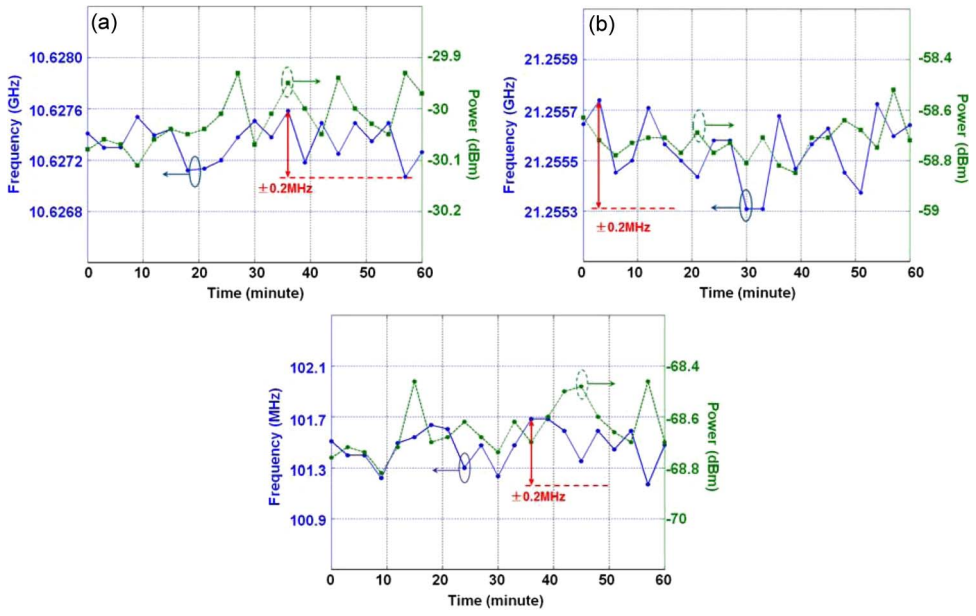

Fig. 6. Stability of the beat frequencies of (a) $\nu_{11}-\nu_P$, (b) $\nu_{21}-\nu_P$, and (c) $\nu_{34}-\nu_{31}$ at an REF temperature of 20 °C and an FUT temperature of 50 °C, with the data measured every 3 min in 1 h.

the ESA with a 1 Hz frequency resolution for a REF temperature of 20 °C and an FUT temperature of 50 °C (shown in Fig. 7). According to (4) and the configuration of the MW-BEFL, the linewidth of the first-order Stokes wavelength is approximately two orders-of-magnitude narrower

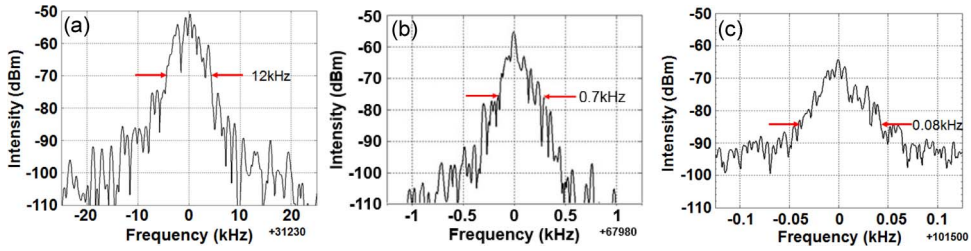

Fig. 7. Beat frequency linewidth measurement of (a) $f_1 = 31.23$ MHz, (b) $f_2 = 67.98$ MHz, and (c) $\nu_{34} - \nu_{31} = 101.5$ MHz.

than that of the pump. The linewidth is observed at the -20 dB points, which is related to the laser real linewidth by $2\sqrt{99}$ times [28]. The -20 dB linewidth points of the frequencies f_1, f_2, and $\nu_{34} - \nu_{31}$, shown in Fig. 7(a)–(c), are 12 kHz, 0.7 kHz, and 0.08 kHz, respectively. Thus, 0.6 kHz, 0.035 kHz, and 0.004 kHz real linewidths are obtained for f_1, f_2, and $\nu_{34} - \nu_{31}$, respectively. The results are in good agreement with our analysis. Therefore, according to (5), the temperature resolution corresponds to approximately 6×10^{-4} °C, 1.8×10^{-5} °C, and 1.3×10^{-6} °C for f_1, f_2, and $\nu_{34} - \nu_{31}$, respectively, depending on the temperature sensitivity of the different order Stokes wavelength.

4. Conclusion

In conclusion, a MW-BEFL sensor with a FUT of 50 m of SMF and a REF of 100 m of SMF for temperature measurement was proposed and demonstrated. The sensitivities of the first-order, second-order and third-order Stokes wavelengths are obtained with different EDFA powers of 250 mW, 500 mW, and 600 mW, respectively, measured for different FUT temperatures from 20 °C to 50 °C at a step of 5 °C. The temperature elevation sensitivity is approximately 1.036 MHz/°C for the first-order Stokes wavelength, 2.006 MHz/°C for the second-order Stokes wavelength and 3.104 MHz/°C for the third-order Stokes wavelength. The experimental results are in good agreement with theory. In addition, with the configuration that uses the FFP filter, the SLM status of every Stokes wavelength is guaranteed. Thus, a less than 0.2 °C temperature error, which corresponds to the resolution of the temperature controller, is obtained in the long-term. Moreover, an approximately 10^{-6} °C temperature resolution at the third-order Stokes wavelength is acquired in the short-term, according to the linewidth of the beat frequency. Furthermore, if we consider that, in this scheme, the HNLF (high nonlinear optical fiber), which can obtain more Stokes wavelengths with a uniform intensity distribution, and a temperature chamber with better resolution are adopted, higher temperature sensitivity and resolution can be obtained by detecting a higher order Stokes wavelength.

References

[1] D. Kersey *et al.*, "Fiber grating sensors," *J. Lightw. Technol.*, vol. 15, no. 8, pp. 1442–1463, Aug. 1997.
[2] K. T. V. Grattan and T. Sun, "Fiber optic sensor technology: An overview," *Sens. Actuators A, Phys.*, vol. 82, no. 1, pp. 40–61, May 2000.
[3] G. H. Ames and J. M. Maguire, "Erbium fiber laser accelerometer," *IEEE Sens. J.*, vol. 7, no. 4, pp. 557–561, Apr. 2007.
[4] J. P. F. Wooler, B. Hodder, and R. I. Crickmore, "Acoustic properties of a fibre-laser microphone," *Meas. Sci. Technol.*, vol. 18, no. 3, pp. 884, Mar. 2007.
[5] X. Yang, S. Luo, Z. Chen, J. H. Ng, and C. Lu, "Fiber Bragg grating strain sensor based on fiber laser," *Opt. Commun.*, vol. 271, no. 1, pp. 203–206, Mar. 2007.
[6] H. Ahmad, A. A. Latif, M. Z. Zulkifli, N. A. Awang, and S. W. Harun, "Temperature sensing using frequency beating technique from single-longitudinal mode fiber laser," *IEEE Sens. J.*, vol. 12, no. 7, pp. 2496–2500, Jul. 2012.
[7] J. Mandal *et al.*, "Bragg grating-based fiber-optic laser probe for temperature sensing," *IEEE Photon. Technol. Lett.*, vol. 16, no. 1, pp. 218–220, Jan. 2004.
[8] J. Mandal *et al.*, "Bragg grating tuned fiber laser system for measurement of wider range temperature and strain," *Opt. Commun.*, vol. 244, no. 1, pp. 111–121, Jan. 2005.

[9] Z. Yin *et al.*, "Fiber ring laser sensor for temperature measurement," *J. Lightw. Technol.*, vol. 28, no. 23, pp. 3403–3408, Dec. 2010.
[10] S. Liu *et al.*, "Multilongitudinal mode fiber laser for strain measurement," *Opt. Lett.*, vol. 35, no. 6, pp. 835–837, Mar. 2010.
[11] J. Mandal *et al.*, "A parallel multiplexed temperature sensor system using Bragg-grating-based fiber lasers," *IEEE Sens. J.*, vol. 6, no. 4, pp. 986–995, Aug. 2006.
[12] A. T. Alavie, S. E. Karr, A. Othonos, and R. M. Measures, "A multiplexed Bragg grating fiber laser sensor system," *IEEE Photon. Technol. Lett.*, vol. 5, no. 9, pp. 1112–1114, Sep. 1993.
[13] X. P. Yang, J. L. Gan, S. H. Xu, and Z. M. Yang, "Temperature sensing based on a Brillouin fiber microwave generator," *Laser Phys.*, vol. 23, no. 4, Feb. 2013, Art. ID. 045104.
[14] Y. J. Song, L. Zhan, S. Hu, Q. H. Ye, and Y. X. Xia, "Tunable multiwavelength Brillouin–erbium fiber laser with a polarization-maintaining fiber Sagnac loop filter," *IEEE Photon. Technol. Lett.*, vol. 16, no. 9, pp. 2015–2017, Sep. 2004.
[15] D. S. Lim *et al.*, "Generation of multiorder Stokes and anti-Stokes lines in a Brillouin erbium-fiber laser with a Sagnac loop mirror," *Opt. Lett.*, vol. 23, no. 21, pp. 1671–1673, Nov. 1998.
[16] Y. G. Shee, M. H. Al-Mansoori, A. Ismail, S. Hitam, and M. A. Mahdi, "Multiwavelength Brillouin–erbium fiber laser with double-Brillouin-frequency spacing," *Opt. Exp.*, vol. 19, no. 3, pp. 1699–1706, Jan. 2011.
[17] M. H. Al-Mansoori, M. K. Abdullah, B. M. Ali, and M. A. Mahdi, "Hybrid Brillouin/erbium fibre laser in a linear cavity for multi-wavelength communication systems," *Opt. Laser Technol.*, vol. 37, no. 5, pp. 387–390, Jul. 2005.
[18] W. Peng *et al.*, "Tunable self-seeded multiwavelength Brillouin–erbium fiber laser using an in-line two-taper Mach–Zehnder interferometer," *Opt. Laser Technol.*, vol. 45, pp. 348–351, Feb. 2013.
[19] Y. Huang, W. Zhang, X. Feng, Y. Huang, and J. Peng, "Bi-directional dual-wavelength Brillouin lasing in a hybrid fiber ring cavity," *Opt. Commun.*, vol. 282, no. 14, pp. 2990–2994, Jul. 2009.
[20] V. L. Iezzi, S. Loranger, M. Marois, and R. Kashyap, "High-sensitivity temperature sensing using higher-order Stokes stimulated Brillouin scattering in optical fiber," *Opt. Lett.*, vol. 39, no. 4, pp. 857–60, Feb. 2014.
[21] R. Xu and X. Zhang, "Multiwavelength Brillouin–Erbium fiber laser temperature sensor with tunable and high sensitivity," *IEEE Photon. J.*, vol. 7, no. 3, pp. 1–8, Jun. 2015.
[22] P. Nicati, K. Toyama, S. Huang, and H. Shaw, "Temperature effects in a Brillouin fiber ring laser," *Opt. Lett.*, vol. 18, no. 24, pp. 2123–2125, Dec. 1993.
[23] T. Kurashima, T. Horiguchi, and M. Tateda, "Thermal effects of Brillouin gain spectra in single-mode fibers," *IEEE Photon. Technol. Lett.*, vol. 2, no. 10, pp. 718–720, Oct. 1990.
[24] Y. Liu, J. L. Yu, W. R. Wang, H. G. Pan, and E. Z. Yang, "Single longitudinal mode Brillouin fiber laser with cascaded ring Fabry–Pérot resonator," *IEEE Photon. Technol. Lett.*, vol. 26, no. 2, pp. 169–172, Jan. 2014.
[25] F. F. Wei, X. F. Yang, Z. R. Tong, Y. Cao, and H. G. Pan, "Dual-wavelength narrow-linewidth fiber laser based on F–P fiber ring filter," *Optik*, vol. 123, no. 11, pp. 1026–1029, Jun. 2012.
[26] A. Debut, S. Randoux, and J. Zemmouri, "Linewidth narrowing in Brillouin lasers: Theoretical analysis," *Phys. Rev. A*, vol. 62, no. 2, 2000, Art. ID. 023803.
[27] T. Kurashima, T. Horiguchi, H. Ohno, and H. Izumita, "Strain and temperature characteristics of Brillouin spectra in optical fibers for distributed sensing techniques," in *Proc. 24th Eur. Conf. Opt. Commun.*, Sep. 1998, vol. 1, pp. 149–150.
[28] C. Spiegelberg *et al.*, "Low-noise narrow-linewidth fiber laser at 1550 nm (June 2003)," *J. Lightw. Technol.*, vol. 22, no. 1, pp. 57–62, Jan. 2004.